Resonance Raman Studies Indicate a Unique Heme Active Site in Prostaglandin H Synthase†

Bih-Show Lou,‖ Jennifer K. Snyder,§ Paul Marshall,§ Jinn-Shyan Wang,‡,# Gang Wu,‡ Richard J. Kulmacz,‡ Ah-Lim Tsai,*,‡ and Jianling Wang*,§

Novartis Pharmaceuticals Corporation, 556 Morris Avenue, Summit, New Jersey 07901, USA, University of Texas Houston Medical School, 6431 Fannin, Houston, Texas 77030, USA, and Chang Gung University, Tao-Yuan 333, Taiwan, ROC

Received June 1, 2000

ABSTRACT: Prostaglandin H synthase isoforms 1 and 2 (PGHS-1 and -2) catalyze the first two steps in the biosynthesis of prostaglandins. Resonance Raman spectroscopy was used to characterize the PGHS heme active site and its immediate environment. Ferric PGHS-1 has a predominant six-coordinate high-spin heme at room temperature, with water as the sixth ligand. The proximal histidine ligand (or the distal water ligand) of this hexacoordinate high-spin heme species was reversibly photolabile, leading to a pentacoordinate high-spin ferric heme iron. Ferrous PGHS-1 has a single species of five-coordinate high-spin heme, as evident from ν_2 at 1558 cm^{-1} and ν_3 at 1471 cm^{-1}. ν_4 at 1359 cm^{-1} indicates that histidine is the proximal ligand. A weak band at 226−228 cm^{-1} was tentatively assigned as the Fe−His stretching vibration. Cyanoferric PGHS-1 exhibited a ν_{Fe-CN} line at 446 cm^{-1} and δ_{Fe-C-N} at 410 cm^{-1}, indicating a "linear" Fe−C−N binding conformation with the proximal histidine. This linkage agrees well with the open distal heme pocket in PGHS-1. The ferrous PGHS-1 CO complex exhibited three important marker lines: ν_{Fe-CO} (531 cm^{-1}), δ_{Fe-C-O} (567 cm^{-1}), and ν_{C-O} (1954 cm^{-1}). No hydrogen bonding was detected for the heme-bound CO in PGHS-1. These frequencies markedly deviated from the ν_{Fe-CO}/ν_{C-O} correlation curve for heme proteins and porphyrins with a proximal histidine or imidazolate, suggesting an extremely weak bond between the heme iron and the proximal histidine in PGHS-1. At alkaline pH, PGHS-1 is converted to a second CO binding conformation (ν_{Fe-CO}: 496 cm^{-1}) where disruption of the hydrogen bonding interactions to the proximal histidine may occur.

Prostaglandin H synthase (PGHS, also known as cyclooxygenase or COX)[1] catalyzes the first two steps in the biosynthesis of prostaglandins (PGs). In these processes, PGHS serves as a bifunctional enzyme that oxidizes arachidonic acid to peroxide prostaglandin G_2 (PGG_2) via its cyclooxygenase activity and reduces PGG_2 to the alcohol prostaglandin H_2 (PGH_2) via its peroxidase activity (*1*−*3*). PGH_2 is the precursor of prostaglandins, prostacyclins, and thromboxanes (*4*). Two isoforms of PGHS have been discovered thus far: PGHS-1 and PGHS-2. The former is constitutively expressed in most cells and tissues as a "housekeeping" enzyme and is believed to play an important role in normal stomach and renal functions. In contrast, PGHS-2 is inducible in a variety of cell types and its synthesized products are believed to participate in inflammation, mitogenesis, and reproduction (*4*−*6*). Enormous efforts have recently been devoted to the structural elucidation of both isozymes and to search for PGHS-2-selective inhibitors (*7*−*11*). These inhibitors form a new generation of nonsteroidal antiinflammatory drugs (NSAIDs) with significantly reduced gastrointestinal toxicity (*88*−*89*).

PGHS-1 is a homodimer of 70-kDa subunits, each with three domains: an epidermal growth factor-like domain, a membrane-binding domain, and a catalytic domain (*7*, *12*). The catalytic domain contains a heme prosthetic group at the peroxidase active site and a physically distinct cyclooxygenase active site (*7*). The cyclooxygenase active site is in an elongated hydrophobic channel (8 × 25 Å) extending from the protein surface (membrane-binding domain) toward the peroxidase active site. The peroxidase active site has a heme coordinated to the protein by His-388 as the proximal ligand in a cavity that is relatively open and exposed to the solvent. Gln-203 and His-207 on the distal side of heme are structurally conserved in other peroxidases, but in PGHS-1 these residues are too far away from the heme iron for direct coordination (*7*). Tyr-385 lies between the heme and the

† This work is partially supported by PHS Grants GM44911 (A.L.T.), GM 52170 (R.J.K.), and NSC 89-2113-M-182-001 (B.S.L.).

* To whom correspondence should be addressed. Jianling Wang, phone: (908) 277-4649, fax: (908) 277-4435, e-mail: jianling.wang@pharma.novartis.com; Ah-Lim Tsai, phone: (713) 500-6771, fax: (713) 500-6810, e-mail: Ah-Lim.Tsai@uth.tmc.edu.

§ Novartis Pharmaceuticals Corporation.

‡ University of Texas Medical School at Houston.

‖ Chang Gung University, Tao-Yuan 333, Taiwan, ROC.

Present address: Department of Public Health, College of Medicine, Fu Jen Catholic University, 510 Chung-Cheng Rd., Hsinchuang, Taipei Hsien, Taiwan 24205.

[1] Abbreviations: 5C/HS, pentacoordinate high-spin; 6C/HS, hexacoordinate high-spin; 6C/LS, hexacoordinate low-spin; CCD, charge-coupled device; CCP, cytochrome *c* peroxidase; CCO, cytochrome *c* oxidase; CPO, chloroperoxidase; EPR, electron paramagnetic resonance; Hb, hemoglobin; HbI, *Scapharca inaequivalvis* hemoglobin; HHO, heme−heme oxygenase complex; HRP, horseradish peroxidase; LPO, lactoperoxidase; Mb, myoglobin; MCD, magnetic circular dichroism; MPO, myeloperoxidase; NOS, nitric oxide synthase; P-450, cytochrome P-450; PGHS, prostaglandin H synthase; RR, resonance Raman; sGC, soluble guanylate cyclase.

10.1021/bi001257c CCC: $19.00
Published on Web 09/12/2000

binding site for fatty acid substrate, in the structural conjunction of the two active sites. Heme is essential for both activities of the enzyme (*1*, *13*) and the characterization of the structure of the heme group and its immediate environment will be of great help in the understanding of the PGHS-1 catalytic mechanism.

Extensive spectroscopic studies have been carried out to characterize the active site structure of PGHS-1 (*14*−*16*) and to investigate the identity and the chemical competence of the tyrosyl residue proposed to be involved in cyclooxygenase catalysis (*2*, *13*). While ferric high-spin heme iron was suggested by the optical absorption study (*14*), EPR and MCD data revealed a mixture of high-spin and low-spin heme coordination states (*15*−*16*).

Resonance Raman (RR) spectroscopy has proved useful for structural characterization of heme and its immediate environment in hemeproteins (*17*). Tsai et al. (*16*) first reported the existence of a mixture of hexacoordinate high-spin (6C/HS) and low-spin heme species (6C/LS). Gaspard et al. (*18*) suggested that the PGHS-1 heme/protein ratio might affect the heme ligation states. The heme active site structure and its immediate environment of PGHS-1 in solution are yet to be well-established. Herein, we report the RR spectra of ligand-free forms of PGHS-1 in ferric and ferrous states, as well as the CO and CN adducts. Our results revealed a heme environment in PGHS-1 that is unusual among hemeproteins with histidine ligands.

MATERIALS AND METHODS

PGHS-1 was purified from ovine seminal vesicles (*19*), and the holoenzyme was prepared by replenishing with heme (*20*). The samples used for this study had cyclooxygenase specific activities in the range of 80−120 μmol of O_2 min^{-1} mg^{-1}.

Samples for RR measurements contained 50−200 μM PGHS-1 (ϵ_{410} = 165 mM^{-1} cm^{-1}) in 0.1 M potassium phosphate buffer (pH 7.2) with 0.1% Tween-20 and 10% glycerol. In pH-dependent experiments, 0.1 M potassium phosphate buffer was utilized for pH 7.2 and 8.5, and a mixture of 0.05 M potassium phosphate and 0.05 M 3-(cyclohexylamino)-1-propanesulfonic acid (Sigma) was used for pH 10.0 and 11.5, each of which contained 5−10% glycerol and 0.1% Tween-20. Ferrous PGHS-1 was obtained by adding ~30-fold excess of a fresh solution of sodium dithionite (Sigma) to the ferric enzyme under anaerobic conditions. The ferric cyanide adduct was prepared by adding about 100 equiv of potassium cyanide (Sigma) to the ferric enzyme, with a later addition of 40 equiv of sodium dithionite for the cyanoferrous PGHS-1 complexes. In the $H_2{}^{18}O$- and D_2O-substitution experiments, an aliquot of concentrated PGHS-1 (~400 μM) was diluted in buffer prepared with $H_2{}^{16}O$, D_2O (Aldrich, >95% isotopic enrichment), or $H_2{}^{18}O$ (ICON, >95% isotopic enrichment) to give final isotopic substitution of hydrogen or oxygen in water of about 90%. The PGHS-1 CO-complex was prepared by an addition of $^{12}C^{16}O$ (Matheson, >99% purity), $^{13}C^{16}O$, $^{12}C^{18}O$, or $^{13}C^{18}O$ gas (ICON, 99%/99% labeled) to ferrous samples under anaerobic conditions. All of the reagents in the present study were used without further purification.

RR spectra were recorded with a custom-built instrument. Sample aliquots (~12 μL) were sealed in a specially designed Raman cell rotating at about 1000 rpm. In most experiments (except for the power-dependent studies), low laser power (0.09−1.8 mW) was utilized to minimize photoinduced heme reduction (*21*), sample denaturation (*22*−*23*), and alterations of ligand binding conformation (*24*). Ferric and ferrous PGHS-1 and their ligand complexes exhibited Soret bands in the 410−432 nm range (Figure 1). Thus, the 413.1-nm line from a krypton ion laser (Coherent) was utilized routinely for the RR studies to achieve better resonance enhancement. Additionally, the 441.6-nm line from a He−Cd laser (Kimmon) was used for ferrous PGHS-1. Scattered light was dispersed by a 1-m spectrograph with a holographic grating (2400 groove/mm) and detected by a CCD camera (Instrument S. A.). Raman shift frequencies were calibrated against lines from indene (Aldrich) (150−1800 cm^{-1}), acetone (Aldrich) (1709.7 cm^{-1}), and potassium ferrocyanide (Aldrich) (2056.7 and 2091.7 cm^{-1}). Some spectra were baseline-corrected, but none were smoothed. Optical absorption spectra were recorded on a Shimadzu UV−Vis spectrophotometer, both prior to and after each Raman measurement to verify sample identity and stability.

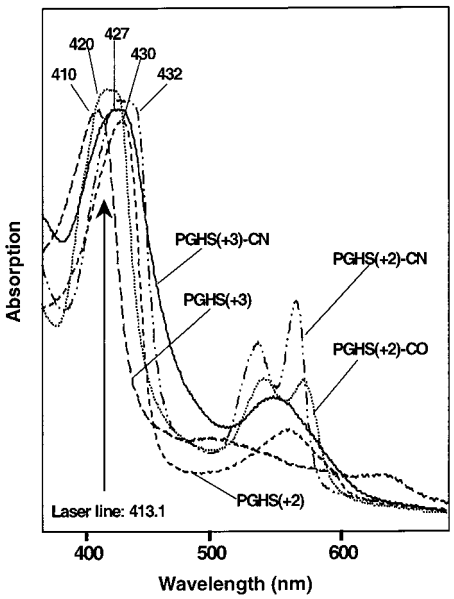

FIGURE 1: Optical absorption spectra of PGHS-1 (~100 μM in 0.1 M potassium phosphate at pH 7.2 containing 0.1% Tween-20 and 10% glycerol): resting ferric (broken line); ferric cyanide adduct (solid line); ferrous (dashed line); ferrous cyanide adduct (dashed−dotted line); ferrous CO-bound form (dotted line).

RESULTS

RR spectra in the high-frequency region for ferric and ferrous PGHS-1 and their CN and CO complexes are shown in Figure 2. The PGHS-1 data are compared with those from other heme-containing proteins and porphyrin model compounds (Table 1). The heme iron oxidation state marker (ν_4), the ligation state marker (ν_3), and two other Raman lines susceptible to the heme spin state and coordination (ν_2 and ν_{10}) were used to characterize the heme active site structure in PGHS-1. For instance, Raman shifts of ν_3 reflect the coordination details of heme iron (Table 1). For a ferric heme iron, ν_3 always positions around 1487−1495 cm^{-1} for pentacoordinate high-spin (5C/HS), 1477−1483 cm^{-1} for 6C/HS, and 1501−1510 cm^{-1} for 6C/LS. In the ferrous form, ν_3 appears near 1465−1473 cm^{-1} for 5C/HS and 1493−

Table 1: Resonance Raman Data (in cm^{-1}) for PGHS-1 and Other Heme Proteins and Models

	Fe^{3+}					Fe^{2+}					
proteins	ν_4	ν_3	ν_2	ν_{10}	heme structure	ν_4	ν_3	ν_2	ν_{10}	heme structure	refs
HHO	1372	1482	1564	1622	6C/HS	1354	1471	1561	1620	5C/HS	(*37*, *62*)
Mb	1370	1481	1563	1620	6C/HS	1356	1473	1564	1617	5C/HS	(*37*, *62*)
LPO	1371	1483	1554	1616	6C/HS	1357	1471	1563		5C/HS	(*36*)
Mb−F	1372	1482	1566	1622	6C/HS						(*63*)
CCP−F	1369	1477	1561	1617	6C/HS						(*64*)
models	1373	1482	1572	1615	6C/HS						(*65*)
PGHS-1	**1370**	**1480**	**1556**	**1620**	**6C/HS**	**1359**	**1471**	**1558**	**1618**	**5C/HS**	(*16*, *18*, this work)
CCP	1371	1494	1570	1629	5C/HS	1356	1471	1563	1618	5C/HS	(*39*, *64*)
HRP	1373	1498	1573	1630	5C/HS	1356	1470		1620	5C/HS	(*63*)
catalase	1373	1489	1574	1625	5C/HS						(*66*)
HbI		1492	1573	1625	5C/HS						(*67*)
sGC	1370	1495	1573	1625	5C/HS	1358	1471	1562	1606	5C/HS	(*68*−*70*)
P-450cam	1368	1488	1570	1623	5C/HS	1345	1466	1564	1601	5C/HS	(*22*)
NOS	1370	1487	1574	1623	5C/HS	1347	1465		1617	5C/HS	(*71*)
CPO	1369	1490	1564	1627	5C/HS	1348	1471	1564	1612	5C/HS	(*72*)
models	1374	1492	1581	1632	5C/HS	1357	1473	1578	1607	5C/HS	(*65*)
NOS ($-BH_4$)	1371	1501	1573	1634	6C/LS						(*82*)
CCP−CN	1372	1506	1579	1638	6C/LS	1360	1495	1580	1629	6C/LS	(*39*, *64*)
CCP−Imd	1375	1505	1579	1635	6C/LS	1361	1495	1584	1627	6C/LS	(*21*, *39*)
models	1374	1506	1590	1642	6C/LS	1360	1493	1587	1615	6C/LS	(*65*)
PGHS-1-CN	**1372**	**1503**	**1584**	**1638**	**6C/LS**	**1360**	**1493**	**1584**	**1623**	**6C/LS**	this work
CCP−CO						1372	1496	1577	1629	6C/LS	(*58*, *73*)
Mb−CO						1372	1501	1585		6C/LS	(*37*)
HHO−CO						1372	1497	1583	1628	6C/LS	(*37*)
PGHS-1−CO						**1373**	**1499**	**1581**	**1626**	**6C/LS**	this work

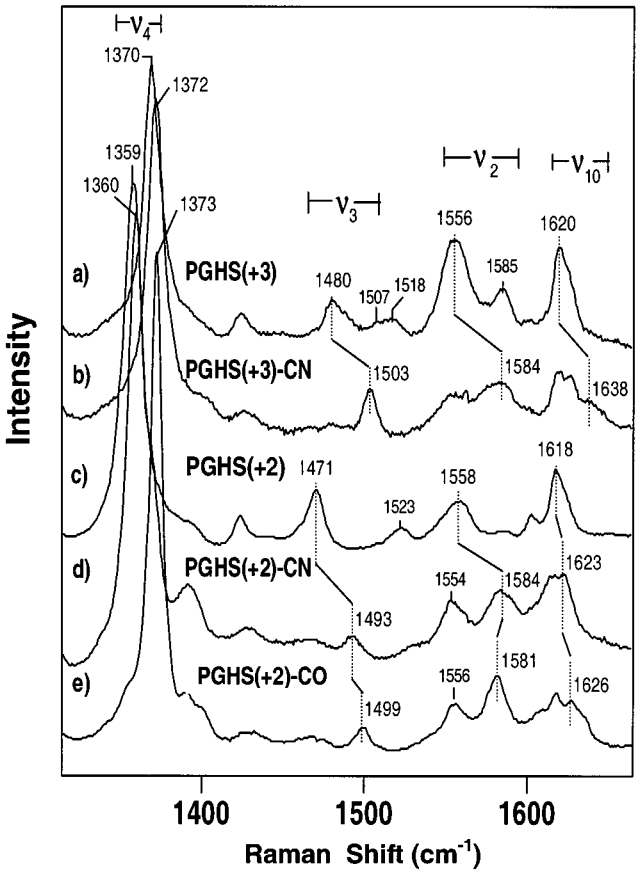

FIGURE 2: High-frequency RR spectra for PGHS-1 (~100 μM in 0.1 M potassium phosphate at pH 7.2 containing 0.1% Tween-20 and 10% glycerol) in the ferric (a and b) and ferrous (c−e) forms: (a) ferric PGHS-1; (b) ferric PGHS-1−CN; (c) ferrous PGHS-1; (d) ferrous PGHS-1−CN; and (e) ferrous PGHS-1−CO. Spectra were recorded at low laser power (0.09−1.8 mW) with the 413.1-nm excitation.

1502 cm^{-1} for 6C/LS. Concurrent shifts also exist for ν_2 (5C/HS: ~1573 cm^{-1}; 6C/HS: ~1560 cm^{-1} and 6C/LS: ~1580 cm^{-1} for the ferric form and 5C/HS: ~1560 cm^{-1} and 6C/LS: ~1580 cm^{-1} for the ferrous form) and ν_{10} (5C/HS: ~1627 cm^{-1}; 6C/HS: ~1620 cm^{-1}; and 6C/LS: ~1638 cm^{-1} for the ferric form and 5C/HS: 1601−1620 cm^{-1} and 6C/LS: 1615−1630 cm^{-1} for the ferrous form) (Table 1 and ref *91*). We found ν_3 at 1480 cm^{-1} for ferric PGHS-1 (trace 2a), thereby suggesting a predominant 6C/HS heme. In addition, two lines (1556 and 1620 cm^{-1}, respectively) that appear in the ν_2 and ν_{10} vicinity described above and were thus tentatively assigned as ν_2 and ν_{10} for ferric PGHS-1 are also consistent with a 6C/HS heme iron. It should be noted that although ν_2 may sometimes coincide in frequency with other porphyrin modes such as ν_{11}, ν_{37}, ν_{38}, and ν_{19}, it is in general more intense than those lines due to the favorable resonance enhancement at current excitation wavelength (*90*). Polarization studies will help to confirm the ν_2 and ν_{10} assignments. In addition, we also detected a weak signal at ~1507 cm^{-1} (the shoulder of 1518-cm^{-1} line) and a signal at 1585 cm^{-1}, consistent with ν_3 and ν_2 for some 6C/LS heme population in ferric PGHS-1. The spectrum of cyanoferric PGHS-1 had prominent 6C/LS signals (trace 2b). The ferrous ligand-free form of the enzyme has a single species of 5C/HS heme, as evident from ν_3 at 1471 cm^{-1} and ν_2 at 1558 cm^{-1} (trace 2c). The existence of a single line of ν_4 at 1373 cm^{-1} for the CO complex and the absence of a ν_4 contribution from ferrous 5C/HS heme iron (near 1359 cm^{-1}) convincingly demonstrated that photolysis of bound CO was negligible in the spectrum of ferrous CO-bound complex.

The ferric and ferrous forms of PGHS-1 had distinct features in the low-frequency region (Figure 3). Resting PGHS-1 (6C/HS) in buffer prepared with natural water showed a signal at 493 cm^{-1} (trace 3c), which was tentatively assigned as the stretching mode associated with heme iron−water interaction (*18*). There was no change of the 493-cm^{-1} line, either in intensity or position, upon substitution of $H_2{}^{16}O$ (trace 3c) by $D_2{}^{16}O$ (trace 3d) or $H_2{}^{18}O$ (trace 3e), indicating that the 493-cm^{-1} line did not originate from Fe−OH (or Fe−OH_2) stretching. The PGHS-1 low-frequency Raman spectrum was not grossly perturbed by heme iron reduction

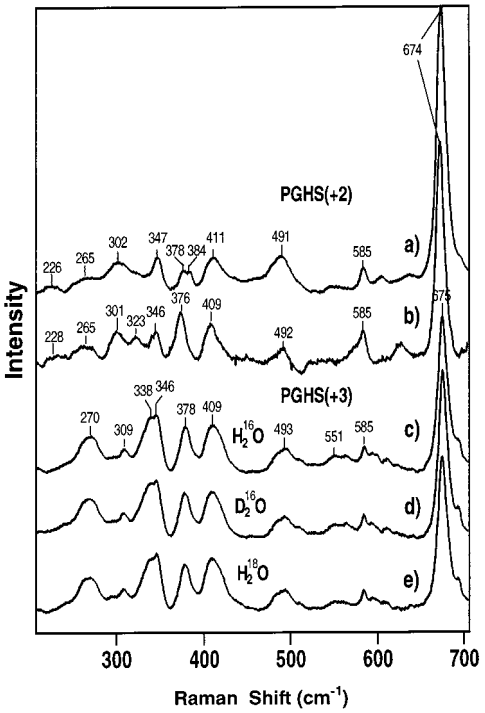

FIGURE 3: Low-frequency RR spectra of PGHS-1 in the ferrous (a−b) and ferric (c−e) forms. Spectra were recorded at low laser power (0.09−1.8 mW) with the 413.1-nm excitation, except that a He−Cd laser (at 441.6 nm) was used to collect spectrum b. (a and b) Dithionite-reduced PGHS-1 in natural water-based buffer; (c−e) ferric PGHS-1 in $H_2{}^{16}O$-based (c), D_2O-based (d), and $H_2{}^{18}O$-based buffers (e).

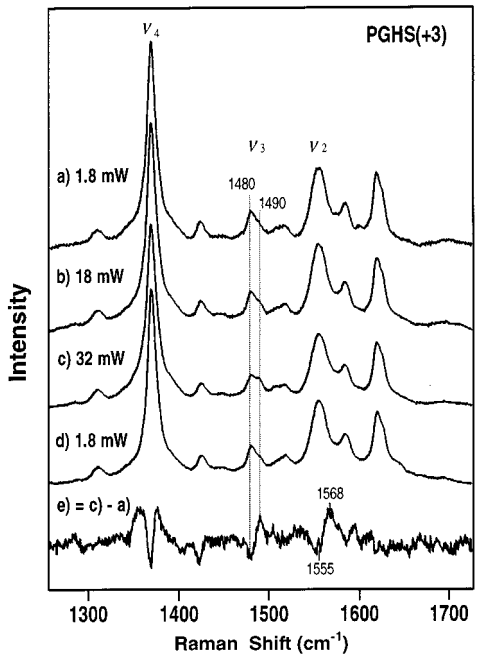

FIGURE 4: Power dependence of ferric PGHS-1 RR spectra: laser power was increased from 1.8 mW (a); to 18 mW (b); to 32 mW (c); and then reduced to 1.8 mW (d). Trace (e) is the difference spectrum between traces (c) and (a). Acquisition sequence: (a), (b), (c) and (d). Other conditions were as described in Figure 2.

(traces 3a and 3b). For instance, the line near 493 cm^{-1} was still present, further proving that this line was not from ν_{Fe-OH_2} for ferric PGHS-1. However, several lines (e.g., 301, 323, 376, and 585 cm^{-1}) were appreciably intensified upon excitation at 441.6 nm (trace 3b). We observed only a weak

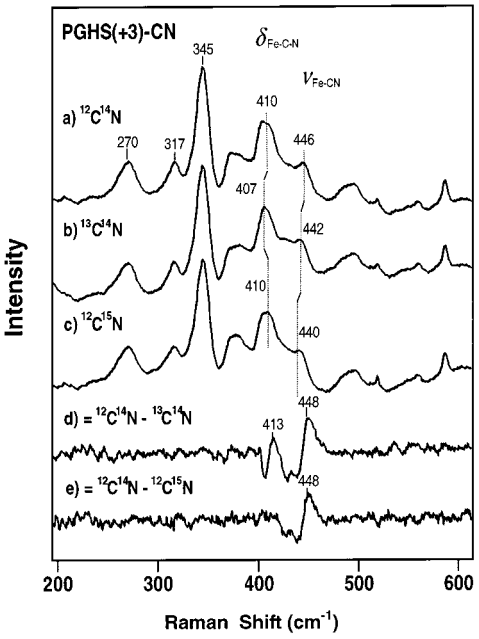

FIGURE 5: RR spectra in the Fe−CN stretching (ν_{Fe-CN}) region for ferric PGHS-1 complexes with $^{12}C^{14}N$ (a), $^{13}C^{14}N$ (b), and $^{12}C^{15}N$ (c). Trace (d) is the difference between spectra (a) and (b), and trace (e) is the difference between spectra (a) and (c). Other conditions were as described in Figure 2.

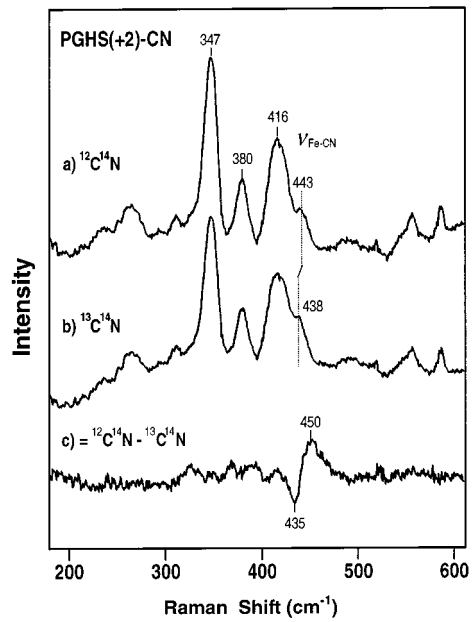

FIGURE 6: RR spectra in the Fe−CN stretching (ν_{Fe-CN}) region for ferrous PGHS-1 complexes with $^{12}C^{14}N$ (a) and $^{13}C^{14}N$ (b). Trace (c) is the difference spectrum between spectra (a) and (b). Other conditions were as described in Figure 2.

band (around 226−228 cm^{-1}) that disappears in the ferrous CN and CO adducts, possibly from the Fe−His stretching mode (ν_{Fe-His}). Surprisingly, neither this 226-cm^{-1} band nor other nearby lines were shifted upon ^{54}Fe or ^{57}Fe substitution of the heme iron, with either 413.1- or 441.6-nm excitation (data not shown).

The high-frequency RR spectral features, in particular ν_3, for ferric PGHS-1 were sensitive to the laser power (Figure 4). For instance, a single ν_3 component was obtained at 1480 cm^{-1} from the 6C/HS sample at 1.8 mW (trace 4a), but a shoulder near 1490 cm^{-1} developed with an increase of the

laser power (traces 4b and 4c). The transition in ν_3 was completely reversible. However, the 1507-cm^{-1} (ν_3) and 1586-cm^{-1} lines (ν_2) of 6C/LS heme were not significantly affected by laser power increases. The difference spectrum (trace 4e) between high power (32 mW) and low power (1.8 mW) conditions revealed ν_3 and ν_2 troughs at 1480 and 1555 cm^{-1} (6C/HS) and peaks at 1490 and 1568 cm^{-1} (5C/HS), respectively. This suggests a photoinduced conversion of the heme iron from 6C/HS to a 5C/HS species, with the heme iron possibly ligated by water or hydroxide as a result of disruption of iron-proximal histidine bonding (Yeh et al., unpublished data). No power-dependence of ν_4 was detected, confirming the absence of the photoinduced heme reduction as compared to the photoreduction occurring in other proteins (*21*).

Multiply labeled cyanide ($^{12}C^{15}N$, $^{13}C^{14}N$, or $^{13}C^{15}N$) helps to establish heme iron−cyanide stretching and bending modes in heme proteins (*25*−*28*, *84*). RR spectra of CN adducts of ferric and ferrous PGHS-1 are shown in Figures 5 and 6. Ferric PGHS-1−CN displayed a line at 446 cm^{-1} (trace 5a) that declined monotonically in frequency to 442 and 440 cm^{-1} with increased CN mass (traces 5b and 5c). In contrast, the line at 410 cm^{-1} (in trace 5a) exhibited a so-called "zigzag" pattern (*84*), shifting in response only to carbon isotope substitution. Although the presence of derivative patterns in both difference spectra (traces 5d and 5e) further suggested the sensitivity of the 446-cm^{-1} line to the overall mass of CN (stretch mode), a derivative feature for the 410-cm^{-1} line appeared only in the $^{12}C^{14}N - {}^{13}C^{14}N$ difference spectrum (trace 5d). We thus attribute the 446-cm^{-1} line, with the "monotonic" isotopic shift, to the Fe−CN stretching vibration (ν_{Fe-CN}) of ferric PGHS-1. The "zigzag" isotopic pattern exhibited by the 410-cm^{-1} line established its assignment as the Fe−C−N bending mode (δ_{Fe-C-N}) (*29*). In contrast to the ferric species, PGHS-1 ferrous CN adducts had only one peak near 443 cm^{-1} that shifted upon isotopic substitution (Figure 6). We tentatively assign it to ν_{Fe-CN} due to the shift (from 443 to 438 cm^{-1}) in response to the single mass change.

At neutral pH, the low-frequency spectra of the PGHS-1 CO adducts showed two CO-associated signals, a strong and sharp line at 531 cm^{-1}, and a weak line at 567 cm^{-1}, both sensitive to CO isotopic substitution (Figure 7). The 531-cm^{-1} line (trace 7a) shifted to 526 cm^{-1} with $^{13}C^{16}O$ (trace 7b), 521 cm^{-1} with $^{12}C^{18}O$ (spectrum 7c), and 517 cm^{-1} with $^{13}C^{18}O$ (trace 7d). This progressive shift was similar to that observed for the CN adducts of ferric PGHS-1 (Figure 5) and for the CO complexes of other heme proteins (*24*), unequivocally establishing this line as the Fe−CO stretching mode (ν_{Fe-CO}). On the other hand, the 567-cm^{-1} line shifted to 550 cm^{-1} with $^{13}C^{16}O$ but moved back to 560 cm^{-1} with $^{12}C^{18}O$ and downshifted to 550 cm^{-1} upon $^{13}C^{18}O$ substitution. Such a "zigzag" pattern of frequency shift is characteristic of an Fe−C−O bending mode (δ_{Fe-C-O}) (*24*).

It should be noted that the shoulder on the 531-cm^{-1} line (near 496 cm^{-1}) showed a slight shift to CO isotopic substitution at neutral pH, as shown in Figure 7. In the difference spectrum (trace 7e) between the $^{12}C^{16}O$ complex spectrum and that of its $^{13}C^{18}O$ adduct, this line, albeit exhibiting a derivative pattern, only represented a small fraction of CO-binding species (~5% that for the 531 cm^{-1}-line). This shows that the 496-cm^{-1} line was mostly

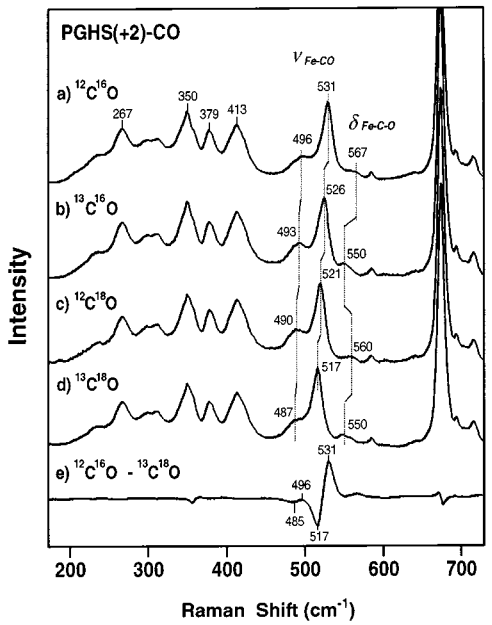

FIGURE 7: RR spectra in the Fe−CO stretching (ν_{Fe-CO}) region of ferrous PGHS-1 complexes with $^{12}C^{16}O$ (a), $^{13}C^{16}O$ (b), $^{12}C^{18}O$ (c), and $^{13}C^{18}O$ (d). Spectrum (e) is the difference between traces (a) and (d). All spectra were recorded at low laser power (0.09−1.8 mW) with the 413.1-nm excitation.

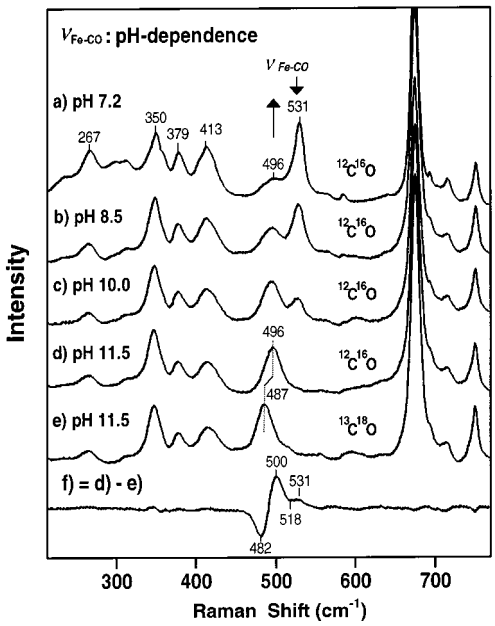

FIGURE 8: pH dependence of the Fe−CO stretching (ν_{Fe-CO}) frequency for ferrous PGHS-1 complexes with $^{12}C^{16}O$ (a−d) and $^{13}C^{18}O$ (e). pH: (a) 7.2; (b) 8.5; (c) 10.0; (d−f) 11.5. Spectrum (f) is the difference between traces (d) and (e). Other conditions were as described in Figure 7.

contributed by a non-CO associated vibration. Indeed, this line was greatly intensified by elevated pH of buffer used (Figure 8) or by utilization of aged PGHS-1 samples (data not shown). At pH 11.5, the 531-cm^{-1} was substantially diminished, showing less than 5% CO-binding population under these conditions (trace 8f). In contrast, the 496-cm^{-1} line became predominant (trace 8d) and also shifted to 487 cm^{-1} upon $^{13}C^{18}O$ substitution (trace 8e), suggesting that it is another Fe−CO stretching mode.

The C−O stretching mode (ν_{C-O}) of heme proteins that always appears in the high-frequency region (1800−2200

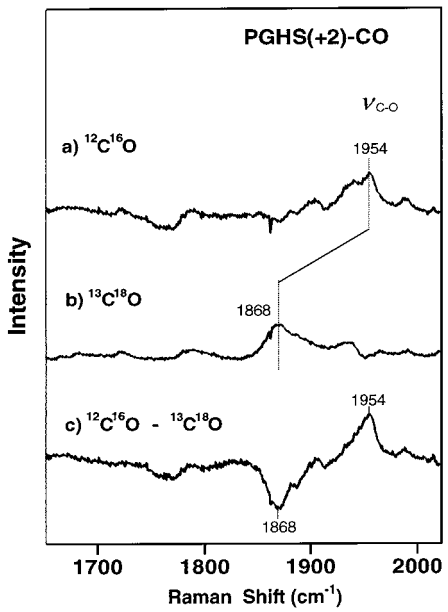

FIGURE 9: RR spectra in the C−O stretching (ν_{C-O}) region of ferrous PGHS-1 complexes with $^{12}C^{16}O$ (a) and $^{13}C^{18}O$ (b). Spectrum (c) is the difference between traces (a) and (b). Other conditions were as described in Figure 7.

cm^{-1}) is considered an IR-active band (*30*−*31*). Establishment of this line by RR spectroscopy offers a number of advantages. First, it allows measurements of all CO-associated marker lines (ν_{Fe-CO}, δ_{Fe-C-O}, and ν_{C-O}) from a single sample for a direct correlation. Second, it requires much less concentrated samples (50−100 μM) than needed for IR experiments. Usually, the detection of ν_{C-O} using Raman is very challenging due to the Raman-inactivity of the line and the problems inherent with higher laser power. A high efficiency CCD camera dramatically improves the quantum efficiency of Raman measurement, thus permitting direct detection of the ν_{C-O} line (as well as other CO-associated lines) with minimal power (e.g., 0.09 mW) (*24*). In the present study, we found a weak peak at 1954 cm^{-1} for the $^{12}C^{16}O$ complex (trace 9a) that shifted to 1868 cm^{-1} upon substitution by $^{13}C^{18}O$ (trace 9b). The shift is obvious in the difference spectrum (trace 8c). We thus assign the line at 1954 cm^{-1} as ν_{C-O} of the PGHS-1 CO adduct. The isotope-dependent shift of this line (88 cm^{-1}) is also in good agreement with those found in other heme proteins (*24*).

DISCUSSION

Heme Coordination of Ferric PGHS-1. RR spectra in the high-frequency region provide information about the coordination, spin state, and π electron density of heme complexes. On the basis of the ν_3 (1480 cm^{-1}) and ν_2 (1556 cm^{-1}) data derived in this study, we conclude that ferric PGHS-1 is dominated by a 6C/HS heme iron, in good agreement with the previous RR, EPR, and MCD studies (*16*, *18*). A 6C/LS heme component was reported earlier in the ferric enzyme (*16*). In our data (Figure 2), the ν_3 shoulder located at 1507 cm^{-1} is still within the range of ν_3 for a 6C/LS heme (1500−1510 cm^{-1}; see Table 1 and ref *32*). In addition, the line at 1585 cm^{-1} in Figure 2 coincides with ν_2 for 6C/LS, confirming the presence of some 6C/LS heme population in ferric PGHS-1. It is noteworthy that coordination of the sixth ligand to ferric heme iron in cytochrome P-450s occurred only in the substrate-free form, where a relatively open distal pocket accounted for the accessibility of water molecules to the heme iron (*33*). The presence of a sixth ligand in ferric PGHS-1 indicates an open distal heme pocket is present in PGHS-1, as observed in crystallographic studies (*7*).

The identity of the distal ligand in the ferric hexacoordinate species of PGHS-1 has yet to be established. Water or OH$^-$ was assigned as the sixth ligand in proteins that possess a 6C/HS ferric heme iron, such as Hb, Mb, LPO, and HHO (*34*−*37*). However, no Fe−water stretch vibration (ν_{Fe-OH_2}) has been identified for the 6C/HS heme structure at neutral pH (using Soret excitation) for direct confirmation of the water ligand. Instead, the presence of a water ligand was inferred by identification of an iron−OH stretching line (ν_{Fe-OH}) when the proteins were transformed into a 6C/LS state at alkaline pH. Water (or a water−His pair) was postulated as the distal ligand of ferric 6C/HS heme iron in PGHS-1 (*16*, *18*). We attempted to identify the Fe−water stretching from 6C/HS heme in ferric PGHS-1 at neutral pH, but none of the RR signals were shifted by either D_2O or $H_2{}^{18}O$ substitution (Figure 3). Despite the lack of distinct ν_{Fe-OH_2} for a 6C/HS heme structure at neutral pH, an unusual pentacoordinate heme configuration was found in ferric PGHS-1 at alkaline pH, where hydroxide was ligated to the ferric heme iron (Yeh et al., unpublished data), thereby suggesting that water was the distal ligand at neutral pH.

Another unusual feature for ferric PGHS-1 is in that one of the axial ligands in the 6C/HS heme species is photolabile. Photoinduced dissociation of endogenous ligands was reported for a 6C/LS species in alkaline ferrous cytochrome *c* peroxidase (*38*−*39*). In that case, the distal ligand, histidine-52, was photolyzed and rapid geminate recombination occurred along with a protein conformational rearrangement (*38*, *40*). PGHS-1 provides an example of photolysis involving a 6C/HS species. In addition, we found that photodissociation of the 6C/HS ligand in PGHS-1 (water or histidine) was fully reversible. The rapid recombination of the photolyzed ligand was in good agreement with dissociation of the proximal histidine from the heme iron, leading to a water-ligated 5C/HS heme iron, as reported in other heme proteins (*41*) or in the alkaline form of ferric PGHS-1 (Yeh et al., unpublished data). However, our current data cannot rule out photolysis of the distal water ligand.

Heme Coordination of Ferrous PGHS-1. Our resonance Raman data (Figure 2) revealed a single 5C/HS species present in ferrous PGHS-1, indicated by ν_3 (1471 cm^{-1}) and ν_2 (1558 cm^{-1}). This 5C/HS ferrous heme was quite stable and did not convert to a 6C/LS species, as was reported earlier (*18*). In the ν_{Fe-His} region (200−270 cm^{-1}) we detected a weak but relatively broad band (226−228 cm^{-1}) that disappeared in the ferrous PGHS-1 complexes with CN$^-$ (Figure 6) and CO (Figure 7). Observation of the line in the 5C/HS ferrous heme but not in the 6C/LS species was consistent with it originating from ν_{Fe-His}, suggesting histidine as the proximal ligand for PGHS-1. It is noteworthy that the weak but broad ν_{Fe-His} band of PGHS-1 is quite anomalous in comparison to other heme-containing proteins. This may be at least in part due to the ineffective resonance enhancement of ν_{Fe-His} in our experiment, as neither of the two laser excitation wavelengths (413.1 and 441.6 nm) used here (traces a and b in Figure 3) is not very close to the

Table 2: ν_{Fe-CN} and δ_{Fe-C-N} Frequencies (in cm^{-1}) for Cyanoferric PGHS-1 and Other Heme Proteins

proteins	linear		bent		refs
	ν_{Fe-CN}	δ_{Fe-C-N}	ν_{Fe-CN}	δ_{Fe-C-N}	
CCO	478	440			(*28*)
Mb (CTT)	453	412			(*84*)
Mb (horse)	452	441			(*28*)
Hb	452	434			(*28*)
SiR−HP	451	390	352	451	(*42*)
LPO (pH 7.0)			360	453	(*44*)
LPO (pH 10.5)			355	452	(*44*)
MPO			361	453	(*25*)
HRP (pH 5.5)	453	405	360	422	(*25*, *45*)
HRP (pH 12.5)	444	405	355	420	(*45*)
CCP (pH 6.5)	457				(*43*)
CCP (pH 10.0)	445	407	355	445	(*43*)
PGHS-1	**446**	**410**			this work
catalase (AN)	435	412	350	456	(*74*)
catalase (BL)	434	413	349	445	(*74*)
P-450 (substrate-free)	413	387	343	434	(*27*)
P-450 (camphor)	416	392	359	424	(*27*)
P-450 (adamantanone)	423	387	357	437	(*27*)

Soret maximum for ferrous PGHS-1 (430 nm). On the other hand, the weak ν_{Fe-His} mode may also implicate an unusual iron-proximal histidine bonding present in PGHS-1 (e.g., weak bonding of the heme iron to an off-axis histidine). Meanwhile, the ν_4 frequency (1359 cm^{-1}) of the ferrous PGHS-1 5C/HS heme also supports a proximal histidine ligand identity (Table 1: 1355−1359 cm^{-1} for histidine or imidazolate, 1345−1348 cm^{-1} for cysteine). This reflects the distinction in the electron donating capability of the atoms involved in the proximal ligation, as electron donation from proximal ligands flows to the π*-antibonding orbital of the heme porphyrin through the central iron (*17*). Collectively, our data confirm the presence of a proximal histidine in PGHS-1 revealed in earlier spectroscopic and crystallographic investigations (*7*, *16*).

Binding Conformation of CN^- Adducts. Cyanoferric derivatives of heme proteins adopt two structurally distinct CN-binding conformations: a "linear" form and a "bent" conformation (*25*, *27*, *42*). In general, diatomic ligands such as CO, CN^-, and NO interact covalently with the heme iron via σ-bonding and π-bonding (*17*, *30*). σ-Bonding requires donations of lone-pair electrons from a ligand σ-orbital or of unpaired electron(s) from a ligand π* orbital to the distal side of the empty d_{z^2} orbital of the heme iron. π-Bonding involves an electron back-donation from heme iron d_π orbitals (d_{xz}, d_{yz}) to the ligand π* orbital. Usually such a π-interaction is favored by "linear" coordination of ligands (e.g., CO). CN^-, albeit isoelectronic with CO, is a better σ-donor but a poorer π-acceptor than CO (*17*, *43*), and thus deviations from the "linear" conformation are more tolerated for CN^- than for CO. As a result, the binding geometry of cyanide is governed to a great extent by the distal environment of the heme active site and varies considerably among hemeproteins (See Table 2). Whereas HRP, CCP, catalase, SiR-HP, and cytochrome P-450 all show both conformations, other proteins possess only one configuration (CCO, Mb, and Hb have a "linear" form; LPO and MPO have a "bent" one).

Recognition of ν_{Fe-CN} and δ_{Fe-C-N} requires multiply isotope-labeled cyanide ligands, with ν_{Fe-CN} manifested by a monotonic shift, whereas δ_{Fe-C-N} exhibits a "zigzag" shift pattern. Such an analysis for cyanoferric PGHS-1 identified the ν_{Fe-CN} (446 cm^{-1}) and the δ_{Fe-C-N} (410 cm^{-1}) frequencies. Using normal coordinate analysis, several groups (*25*, *27*, *42*) further discovered that a higher frequency for ν_{Fe-CN} than for δ_{Fe-C-N} was seen for a "linear" species, whereas a reverse trend with a lower frequency for ν_{Fe-CN} than for δ_{Fe-C-N} was associated with a "bent" Fe−C−N conformation. For the latter, the anomalous appearance of the two modes was attributed to the kinetic mixing occurring in the "bent" conformation (*25*, *44*). By these criteria, ferric PGHS-1-CN adopts a "linear" conformation, as its ν_{Fe-CN} frequency (446 cm^{-1}) is higher than the δ_{Fe-C-N} frequency (410 cm^{-1}). This "linear" Fe−CN conformation implicates an uncrowded distal heme pocket in PGHS-1, in agreement with the PGHS-1 crystal structure (*7*). Cyanide bound in the linear form was found to strongly interact via hydrogen bonding with nearby amino acid residues or water clusters in HRP (*25*, *45*), CCP, (*43*) and P-450 (*27*). Examination of the dependence of ν_{Fe-CN} and δ_{Fe-C-N} on pH and on D_2O substitution should help determine if such hydrogen bonding interactions also exist in ferric PGHS−CN.

The ν_{Fe-CN} frequency is sensitive to the electronic properties of the proximal ligand (*46*). This appears also to be the case for the "linear" cyanoferric adducts of other heme proteins (Table 2). For instance, cytochrome P-450, with a proximal cysteine, has lower ν_{Fe-CN} frequencies (410−425 cm^{-1}) than peroxidases or globins (440−460 cm^{-1}), with a proximal histidine or imidazolate. Catalase, with a proximal tyrosine, exhibited a ν_{Fe-CN} frequency between the two above categories (430−440 cm^{-1}). The appreciably lower ν_{Fe-CN} frequencies in P-450s than in peroxidases or globins should not be surprising. As an excellent σ-donor but a poor π-acceptor, cyanide interacts with the heme iron primarily through σ-bonding to the iron d_{z^2} orbital. Such ligation inescapably competes with the proximal ligand as the two axial ligands utilize the opposite ends of the same iron d_{z^2} orbital. An electron-rich proximal ligand (e.g., cysteine in P-450s) would thus weaken the Fe−CN bond order on the distal side. CCO is unusual among proteins containing proximal histidine with its high ν_{Fe-CN} value (478 cm^{-1}) ascribed to direct interactions with a nearby Cu_B center residing above the bound cyanide (*28*). The ν_{Fe-CN} data (446 cm^{-1}) from our study further confirm the existence of a proximal histidine in PGHS-1.

Binding Conformation of Ferrous CO Adducts. Heme-bound CO-associated vibrations (ν_{Fe-CO}, δ_{Fe-CO}, and ν_{C-O}) are greatly sensitive to the immediate environment of the heme iron and thus widely used to explore heme active site structure (*24*, *30*, *47*−*50*). Carbon monoxide, with 10 valence electrons, is a σ-donor and a π-acceptor when bound to heme iron (see above), allowing the Fe−CO bond order to be correlated with that of C−O. In general, the ν_{Fe-CO} and ν_{C-O} frequencies are dictated by at least three factors. First, the ν_{Fe-CO} and ν_{C-O} frequencies and the correlation between them reflect the identity or properties of the proximal ligand because bound CO competes with the proximal ligand for the same iron d_{z^2} orbital. For instance, CO derivatives of heme proteins or porphyrins with a similar proximal ligand (e.g., histidine or imidazolate) align on the same correlation curve (solid line in Figure 10), whereas those having a proximal thiolate follow a different curve (broken line in Figure 10) (*30*, *47*). Second, the ν_{Fe-CO} and ν_{C-O} frequencies indicate the polarity of the distal heme pocket (*24*, *48*). This

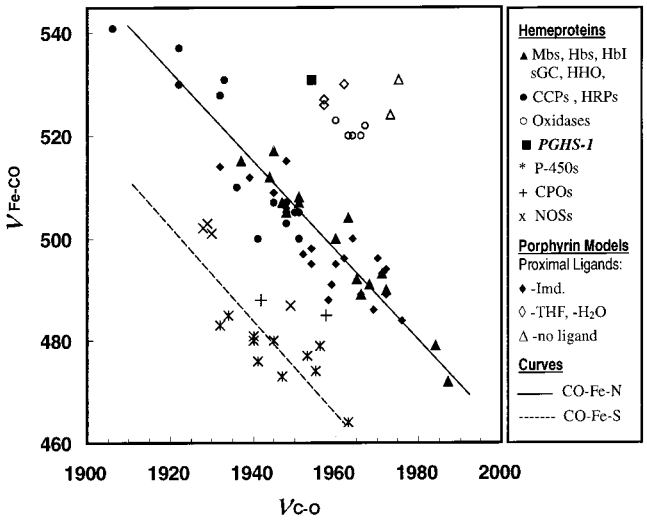

FIGURE 10: Correlation of ν_{Fe-CO}/ν_{C-O} frequency for ferrous CO-adducts of hemeproteins and porphyrin models. The dashed line fits data for proteins with a proximal thiolate ligand (★, P-450s; +, CPOs; x, NOSs), and the solid line fits data for proteins with a nitrogenous proximal ligand (▲, globins or globin-like proteins; ○, oxidases; ●, peroxidases; ◆, porphyrin models; and ■, PGHS-1). Porphyrin models lacking a proximal ligand are denoted by (△) and those with a weak proximal ligand are denoted by (◇).

is because a highly polar environment favors π-back-donation, thereby strengthening the Fe−CO bond order (i.e., increased ν_{Fe-CO}) and weakening the C−O bond strength (i.e., reduced ν_{C-O}) due to increased electron density in the CO antibonding orbital. Third, the frequency correlation sometimes permits exploration of the impact of steric hindrance on heme-bound ligands, with distal steric effects influencing the ν_{Fe-CO} frequency more than that of ν_{C-O} (*49*).

Our current results using multiply labeled CO firmly established ν_{Fe-CO} (531 cm^{-1}) and ν_{C-O} (1954 cm^{-1}) for ferrous PGHS-1 CO adducts at neutral pH (Figures 7 and 9 and Table 3). The ν_{Fe-CO}/ν_{C-O} correlation point for PGHS-1 was surprisingly well above the correlation curve for heme proteins with a proximal histidine (Figure 10), although both crystallographic (Picot et al., 1994) and spectroscopic studies (ref *16* and this work) leave no doubt for histidine as the proximal ligand in ferric and ferrous PGHS-1. We believe that an unusually weak coordination of the proximal ligand is responsible for the anomalous CO-binding features in PGHS-1. Several observations support this contention. First, dissociation of the proximal histidine and formation of a pentacoordinate nitrosyl heme structure were observed for the ferrous−NO complex of PGHS-1 (ref *51* and Lou et al., unpublished data). Such weakening and eventual disruption of the Fe-proximal histidine bond upon coordination of NO on the distal side of heme does not occur for other heme proteins except sGC. Second, crystallographic data suggest that either the histidine plane is tilted away from the heme normal or the N_ϵ of histidine is positioned away from the axial position (*2*, *7*). Because coordination of the proximal ligand to the heme utilizes the iron d_{z^2} orbital along with the heme normal, either of the above two factors would weaken the heme iron-proximal ligand bond order. As a consequence, when CO is bound, it behaves as if a weak proximal ligand were present (e.g., a tyrosine residue or a water molecule). Binding of an electron-rich ligand, such as NO, at the distal side, completely breaks such a weak iron-proximal histidine bond due to direct competition for the iron d_{z^2} orbital. An alternative origin for the unusual PGHS-1 CO-binding characteristics would be proximal coordination by a weak exogenous entity, such as H_2O in a transient form of myoglobin (*52*).

Table 3: ν_{Fe-CO} and ν_{C-O} Frequencies (in cm^{-1}) of PGHS-1 and Other Heme Proteins

proteins	ν_{Fe-CO}	δ_{Fe-C-O}	ν_{C-O}	prox ligand	refs
catalase	542	593		tyrosine	(*61*)
CCP (acidic)	537	589	1922	imidazolate	(*57*−*58*, *73*)
(alkaline)	505		1948	imidazolate	(*58*, *73*)
HRP (pH 7)	541	590	1906	imidazolate	(*60*)
(pH 10)	531		1933	imidazolate	(*60*)
PGHS-1	**531**	**567**	**1954**	**histidine**	this work
CCO (α)	520	578	1964	histidine	(*49*, *53*, *76*, *85*−*86*)
(β)	493			histidine	(*49*, *83*, *87*)
HbI	517	581	1945	histidine	(*77*)
Mb	512	577	1944	histidine	(*75*)
Hb (human)	507	578	1951	histidine	(*75*)
HHO-2	504	573	1963	histidine	(*37*)
sGC	472	562	1987	histidine	(*69*, *78*)
	497	574	1959	histidine	(*68*, *70*)
b-NOS (α)	501		1930	cysteine	(*24*, *71*)
(β)	487	562	1949	cysteine	(*24*, *71*)
CPO	485	560	1958	cysteine	(*24*, *26*)
P450 (α)	480	556	1940	cysteine	(*22*, *80*−*81*)
(β)	464	556	1963	cysteine	(*79*−*80*)

Several other explanations for the anomalous ν_{Fe-CO}/ν_{C-O} correlation in PGHS-1 can probably be eliminated. First, such aberrant behavior was reported in CO derivatives of oxidase superfamily proteins (*47*) and attributed to the existence of a Cu_B binuclear center (*49*, *53*−*54*) immediately above the heme active site (4.5 Å) (*55*−*56*). In PGHS-1, however, such steric hindrance is unlikely because the crystal structure (*9*) and our Raman results (e.g., the "linear" Fe−CN conformation in the PGHS-1 ferric CN adduct) all indicate an open distal pocket in PGHS-1. Second, the intensity of the δ_{Fe-C-O} line is sensitive to the polar environment near the bound CO and to the distortion of the CO-binding geometry away from the heme normal by steric hindrance (*48*). The extremely weak contribution of δ_{Fe-C-O} detected for PGHS-1 in comparison to that of ν_{Fe-CO} argues against strong polar or steric impacts on CO (Figure 7). Our current studies show that ν_{Fe-CO} for PGHS-1 is very high (531 cm^{-1}), which could originate from hydrogen bonding to CO (*18*). It is possible that bound CO hydrogen bonds to nearby distal pocket residues, such as His-207 or Gln-203 (*9*). However, the ν_{C-O} frequency in the PGHS-1 CO complex did not shift upon D_2O substitution (data not shown), in contrast to CCP (*57*) and NOS (Wang et al., unpublished data), arguing against the presence of hydrogen bonding to the heme-bound CO in PGHS-1. Even if such hydrogen bonding interactions exist, they usually cause the ν_{Fe-CO}/ν_{C-O} correlation point to shift along the correlation curve, as found in CCP (*17*, *58*), HRP (*59*−*60*), and NOS (ref *24* and Wang et al., unpublished data), rather than to move off the curve. Thus, hydrogen bonding interactions are very unlikely to account for the sizable deviation of the PGHS-1 ν_{Fe-CO}/ν_{C-O} correlation point. Third, the ν_{Fe-CO}/ν_{C-O} correlation curves (mostly the ν_{Fe-CO} values) of heme proteins and heme models are highly coupled to the electronic properties of the proximal ligand involved. For instance, cysteine-containing proteins (P-450, NOS, and CPO) commonly have weaker ν_{Fe-CO} values than histidine-containing proteins (Table 3). On the other hand,

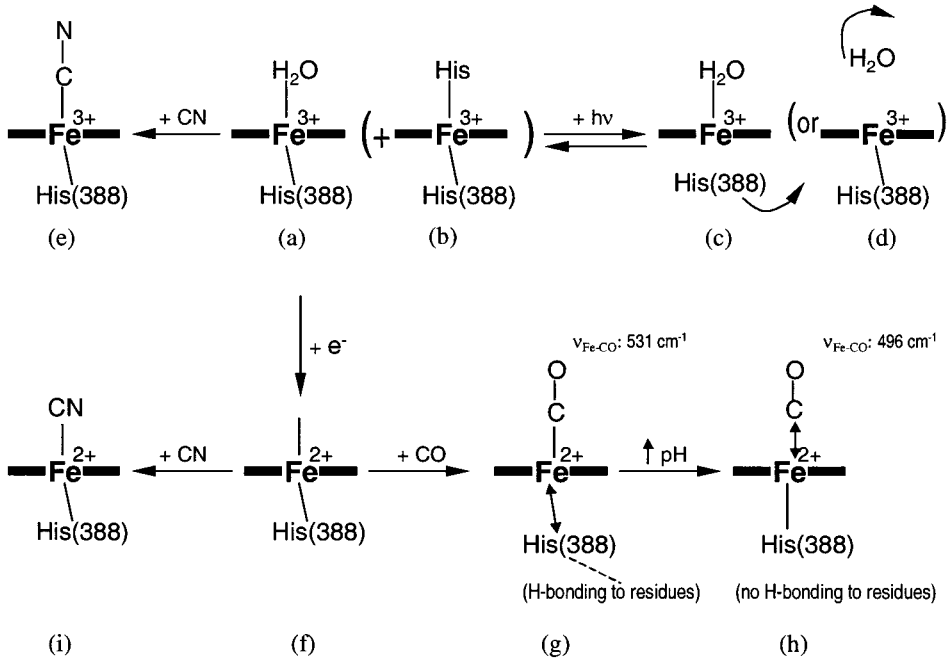

FIGURE 11: Schematic presentation of PHGS-1 heme structures in various forms. (a) Ferric PGHS-1 has a predominant 6C/HS heme iron with water ligated on the distal side. (b) A small fraction of ferric PGHS-1 may exist as 6C/LS heme with bis-histidine ligation. Photolysis of the ferric 6C/HS species gives a 5C/HS species, possibly coordinated with water (c) or histidine (d). (e) Cyanoferric PGHS-1 adopts a "linear" Fe−C−N binding conformation with a proximal histidine. (f) Ferrous PGHS-1 has a single 5C/HS heme structure with a neutral histidine as the proximal ligand. (g) At neutral pH, ferrous PGHS-1 CO-complex has an extremely weak Fe-proximal bonding and stronger Fe−CO bond order. (h) At alkaline pH, PGHS-1 is converted to another CO binding conformation with weaker Fe−CO bonding.

the strongest Fe−CO bond of heme proteins was reported for catalase (ν_{Fe-CO}: 542 cm^{-1}) and was attributed to the poor electron-donating properties of the proximal tyrosine oxygen (*61*). Extensive crystallographic and spectroscopic studies show that a histidine (His-388) is the proximal PGHS-1 ligand, and there is no adjacent tyrosine residue, so a switch of the proximal ligation to a tyrosine residue upon CO coordination, as proposed for other hemeproteins (*47*) can be ruled out for PGHS-1.

We also detected a second Fe−CO binding conformation (ν_{Fe-CO} at 496 cm^{-1}) at alkaline pH or using aged form of PGHS-1 (Figure 8). Lacking evidence to support hydrogen bonding to the heme-bound CO at neutral pH, we postulate that disruption of hydrogen bonding between the proximal histidine and nearby amino acid residues may occur under these conditions. The pH- or age-dependent conversion of the CO-binding conformation of PGHS-1 (from the 531-cm^{-1} form) to the 496-cm^{-1} form was progressive with time and with laser irradiation in the Raman experiments and was irreversible (data not shown). This suggests a conversion possibly to a denatured protein form as a result of conformational perturbations, as found in the low pH Mb (*30*) and the denatured species of P-450 (*22*) and of NOS (*23*). This denatured form is featured by an unconstrained heme pocket where the heme iron was coordinated to a neutral histidine (*22*−*23*). Apparently, such a denatured CO-binding species of PGHS-1 is a very minor component at neutral pH using the current preparation procedure (Figure 7).

In summary, PGHS-1 has primarily a 6C/HS heme in the ferric form (structure a in Figure 11) and a single 5C/HS heme species in the ferrous state (structure f). Water is probably the sixth ligand in ferric 6C/HS PGHS-1, and the proximal histidine is reversibly photolabile, leading to 5C/HS ferric heme iron (Figure 11, structure c). Our data reconfirm histidine as the proximal ligand, consistent with previous studies. The "linear" Fe−C−N binding conformation in cyanoferric PGHS-1 (structure e), indicates an open distal heme pocket, consistent with the crystal structure. The ferrous PGHS-1 CO complex has an unusual CO-binding conformation at neutral pH (ν_{Fe-CO}: 531 cm^{-1} and ν_{C-O}: 1954 cm^{-1}), but no hydrogen bonding was detected for the heme-bound CO in PGHS-1 (Figure 11, structure g), suggesting either an extremely weak bond between the heme iron and the proximal histidine or the presence of a weak external ligand such as water as the proximal ligand. The relatively weak Fe-proximal histidine interactions in PGHS-1 we report here may originate from a tilted histidine from the heme normal or a large deviation of the N_ϵ of histidine from the axial position as implied by the X-ray crystal structure (*2*, *9*). At alkaline pH, PGHS-1 is converted to another CO binding conformation (ν_{Fe-CO}: 496 cm^{-1}) where disruption of the hydrogen bonding to the proximal histidine may occur (Figure 11, structure h).

The open structure of the heme pocket in PGHS-1 revealed in the present study may relate to the wide specificity to peroxide substrates of PGHS (*13*). Substantial evidence supports a branched chain radical mechanism of PGHS with a nonstoichiometric coupling between the peroxidase and the cyclooxygenase activities. Activation of the cyclooxygenase activity only requires very low-level activation of the peroxidase. Thus a wide specificity of the peroxidase heme to various peroxide substrates is advantageous in terms of activation of the cyclooxygenase activity. In contrast, a strict stereospecificity is mandatory for the cyclooxygenase substrate interaction to give the overall enzymatic specificity of PGHS.

While this paper was in preparation, an RR study on flurbiprofen-treated PGHS-1 was in press by Seibold et al.

Except for minor differences, their results show nice agreement with our data obtained from PGHS-1 in the absence of inhibitor. This similarity indicates that flurbiprofen which was claimed to stabilize the PGHS-1 heme does not make a significant difference in the formation of heme complexes with different ligands.

REFERENCES

1. Smith, W. L., Eling, T. E., Kulmacz, R. J., Marnett, L. J., and Tsai, A.-L. (1992) *Biochemistry 31*, 3−7.
2. Ruf, H. H. (1997) in *Bioinorganic Chemistry* (Trautwein, A. X., Ed.) pp 373−384, Wiley-VCH, Bonn.
3. Marnett, L. J., Rowlinson, S. W., Goodwin, D. C., Kalgutkar, A. S., and Lanzo, C. A. (1999) *J. Biol. Chem. 274*, 22903−22906.
4. Vane, J. R., Bakhle, Y. S., and Botting, R. M. (1998) *Annu. Rev. Pharmacol. Toxicol. 38*, 97−120.
5. Williams, C. S., and Dubois, R. N. (1996) *Am. J. Physiol. 270*, G393−400.
6. Jouzeau, J. Y., Terlain, B., Abid, A., Nedelec, E., and Netter, P. (1997) *Drugs 53*, 563−582.
7. Picot, D., Loll, P. J., and Garavito, R. M. (1994) *Nature 367*, 243−249.
8. Filizola, M., Perez, J. J., Palomer, A., and Mauleon, D. (1997) *J. Mol. Graphics Modell. 1*5, 290−300.
9. Picot, D. (1998) in *Lung Biology in Health Disease* (Szczeklik, A., Gryglewski, R. J., and Vane, J. R., Eds.) Vol. 114 (Eicosanoids, Aspirin, and Asthma) pp 161−186, Marcel Dekker, New York.
10. Toh, H., and Tanabe, T. (1998) in *Eicosanoids and Related Compounds in Plants and Animals* (Rowley, A. F., Kuhn, H, and Schewe, T., Eds.) pp 25−46, Princeton University Press, Princeton.
11. Garavito, R. M., and DeWitt, D. L. (1999) *Biochim. Biophys. Acta 1441*, 278−287.
12. Picot, D., Loll, P. J., and Garavito, R. M. (1994) *FEBS Lett. 346*, 21−25.
13. Tsai, A.-L., Wei, C., Baek, H. K., Kulmacz, R. J., and Van Wart, H. E. (1997) *J. Biol. Chem. 272*, 8885−8894.
14. Lambeir, A.-M., Markey, C. M., Dunford, H. B., and Marnett, L. J. (1985) *J. Biol. Chem. 260*, 14894−14896.
15. Karthein, R., Nastainczyk, W., and Ruf, H. H. (1987) *Eur. J. Biochem. 166*, 173−180.
16. Tsai, A.-L., Kulmacz, R. J., Wang, J.-S., Wang, Y., Van Wart, H. E., and Palmer, G. (1993) *J. Biol. Chem. 268*, 8554−8563.
17. Wang, J., Caughey, W. S., and Rousseau, D. L. (1996) in *Methods in Nitric Oxide Research* (Feelisch, M., and Stamler, J., Eds.) pp 427−454, John Wiley and Sons, Chichester.
18. Gaspard, S., Chottard, G., Mahy, J.-P., and Mansuy, D. (1996) *Eur. J. Biochem. 238*, 529−537.
19. Kulmacz, R. J., and Lands, W. E. M. (1987) in *Prostaglandins and Related Substances: A Practical Approach* (Benedetto, C., McDonald-Gibson, R. G., Nigam, S., and Slater, T. F., Eds.) pp 209−227, IRL Press, Washington, DC.
20. Kulmacz, R. J., Palmer, G., Wei, C., and Tsai, A.-L. (1994) *Biochemistry 33*, 5428−5438.
21. Wang, J., Zhu, H., and Ondrias, M. R. (1992) *Biochemistry 31*, 12847−12854.
22. Wells, A. V., Li, P., Champion, P. M., Martinis, S. A., and Sligar, S. G. (1992) *Biochemistry 31*, 4384−4393.
23. Wang, J., Stuehr, D. J., and Rousseau, D. L. (1995) *Biochemistry 34*, 7080−7087.
24. Wang, J., Stuehr, D. J., and Rousseau, D. L. (1997) *Biochemistry 36*, 4595−4606.
25. Lopez-Garriga, J. J., Oertling, W. A., Kean, R. T., Hoogland, H., Wever, R., and Babcock, G. T. (1990) *Biochemistry 29*, 9387−9395.
26. Hu, S., and Kincaid, J. R. (1993) *J. Biol. Chem. 268*, 6189−6193.
27. Simianu, M. C., and Kincaid, J. R. (1995) *J. Am. Chem. Soc. 117*, 4628−4636.
28. Hirota, S., Ogura, T., Shinzawa-Itoh, K., Yoshikawa, S., and Kitagawa, T. (1996) *J. Phys. Chem. 100*, 15274−17279.
29. Benko, B., and Yu, N.-T. (1983) *Proc. Natl. Acad. Sci. U.S.A. 80*, 7042−7046.
30. Yu, N.-T., and Kerr, E. A. (1988) in *Biological Applications of Raman Spectroscopy* (Spiro, T. G., Ed.) Vol. III, pp 39−95, John Wiley and Sons, New York.
31. Sampath, V., Rousseau, D. L., and Caughey, W. S. (1996) in *Methods in Nitric Oxide Research* (Freelisch, M., and Stamler, J., Eds.) pp 413−426, Wiley, Chichester.
32. Spiro, T. G., Stong, J. D., and Stein, P. (1979) *J. Am. Chem. Soc. 101*, 2648−2655.
33. Champion, P. M., Gunsalus, I. C., and Wagner, G. C. (1978) *J. Am. Chem. Soc. 100*, 3743−3751.
34. Asher, S. A., Vickery, L. E., Schuster, T. M., and Sauer, K. (1977) *Biochemistry 16*, 5849−5856.
35. Asher, S. A., and Schuster, T. M. (1979) *Biochemistry 18*, 5377−5387.
36. Manthey, J. A., Boldt, N. J., Bocian, D. F., and Chan, S. I. (1986) *J. Biol. Chem. 261*, 6734−6741.
37. Takahashi, S., Wang, J., and Rousseau, D. L. (1994) *Biochemistry 33*, 5531−5538.
38. Smulevich, G., Miller, M. A., Kraut, J., and Spiro, T. G. (1991) *Biochemistry 30*, 9546−9558.
39. Wang, J., Boldt, N. J., and Ondrias, M. R. (1992) *Biochemistry 31*, 867−878.
40. Wang, J., Larsen, R. W., Chan, S. I., Boldt, N. J., and Ondrias, M. R. (1992) *J. Am. Chem. Soc. 114*, 1487−1488.
41. Das, T. K., Boffi, A., Chiancone, E., and Rousseau, D. L. (1999) *J. Biol. Chem. 274*, 2916−2919.
42. Han, S., Madden, J. F., Siegel, L. M., and Spiro, T. G. (1989) *Biochemistry 28*, 5477−5485.
43. Rajani, C., and Kincaid, J. R. (1995) *J. Raman Spectrosc. 26*, 969−974.
44. Hu, S., Treat, R. W., and Kincaid, J. R. (1993) *Biochemistry 32*, 10125−10130.
45. Al-Mustafa, J., and Kincaid, J. R. (1994) *Biochemistry 32*, 2191−2197.
46. Uno, T., Hatano, K., Nihsimura, Y., and Arata, Y. (1988) *Inorg. Chem. 27*, 3215−3219.
47. Rousseau, D. L., Ching, Y.-C., and Wang, J. (1993) *J. Bioenerg. Biomembr. 25*, 165−176.
48. Ray, G. B., Li, X.-Y., Alers, J. A., Sessler, J. L., and Spiro, T. G. (1994) *J. Am. Chem. Soc. 116*, 162−176.
49. Wang, J., Takahashi, S., Rousseau, D. L., Hosler, J. P., Ferguson-Miller, S., Mitchell, D. M., and Gennis, R. B. (1995) *Biochemistry 34*, 9819−9825.
50. Wang, J., Takahashi, S., and Rousseau, D. L. (1995) *Proc. Natl. Acad. Sci. U.S.A. 92*, 9402−9406.
51. Tsai, A.-L., Wei, C., and Kulmacz, R. J. (1994) *Arch. Biochem. Biophys. 313*, 367−372.
52. Han, S., Ching, Y.-C., and Rousseau, D. L. (1990) *Nature 348*, 89−90.
53. Uno, T., Mogi, T., Tsuboi, M., Nihsimura, Y., and Anraku, Y. (1994) *J. Biol. Chem. 269*, 11912−11920.
54. Hosler, J. P., Ferguson-Miller, S., Callhoun, M. W., Thomas, J. W., Hill, J., Lemieux, L., Ma, J., Georgiou, C., Fetter, J., Shapleigh, J., Tecklenburg, M., Babcock, G. T., and Gennis, R. B. (1993) *J. Bioenerg. Biomembr. 25*, 121−136.
55. Tsukihara, T., Aoyama, H., Yamashita, E., Tomizaki, T., Yamaguchi, H., Shinzawa-Itoh, K., Nakashima, R., Yaono, R., and Yoshikawa, S. (1995) *Science 269*, 1069−1074.
56. Iwata, S., Ostermeier, C., Ludwig, B., and Michel, H. (1995) *Nature 376*, 660−669.
57. Satterlee, J. D., and Erman, J. E. (1984) *J. Am. Chem. Soc. 116*, 1139−1140.
58. Spiro, T. G., Smulevich, G., and Su, C. (1990) *Biochemistry 29*, 4497−4508.
59. Smith, M. L., Ohlsson, P.-I., and Paul, K.-G. (1983) *FEBS Lett. 163*, 303−305.
60. Uno, T., Nishimura, Y., Tsuboi, M., Makino, R., Iizuka, T., and Ishimura, Y. (1987) *J. Biol. Chem. 262*, 4549−4556.
61. Hu, S., and Kincaid, J. R. (1992) *FEBS Lett. 314*, 293−296.

62. Takahashi, S., Wang, J., Rousseau, D. L., Ishikawa, K., Yoshida, T., Host, J. R., and Ikeda-Saito, M. (1994) *J. Biol. Chem. 269*, 1010−1014.
63. Callahan, P. M., and Babcock, G. T. (1981) *Biochemistry 20*, 952−958.
64. Dasgupta, S., Rousseau, D. L., Anni, H., and Yonetani, T. (1989) *J. Biol. Chem. 264*, 654−662.
65. Babcock, G. T. (1988) in *Biological Applications of Raman Spectroscopy* (Spiro, T. G., Ed.) Vol. III, pp 293−346, John Wiley and Sons, New York.
66. Sharma, K. D., Andersson, L. A., Loehr, T. M., Terner, J., and Goff, H. M. (1989) *J. Biol. Chem. 264*, 12772−12779.
67. Boffi, A., Takahashi, S., Spagnuolo, C., and Rousseau, D. L., and Chiancone, E. (1994) *J. Biol. Chem. 269*, 20437−20440.
68. Yu, A. E., Hu, S., Spiro, T. G., and Burstyn, J. N. (1994) *J. Am. Chem. Soc. 116*, 4117−4118.
69. Deinum, G., Stone, J. R., Babcock, G. T., and Marletta, M. A. (1996) *Biochemistry 35*, 1540−1547.
70. Fan, B., Gupta, G., Danziger, R., Friedman, J., and Rouseau, D. L. (1998) *Biochemistry 37*, 1178−1184.
71. Wang, J., Stuehr, D. J., Ikeda-Saito, M., and Rousseau, D. L. (1993) *J. Biol. Chem. 268*, 22255−22258.
72. Remba, R. D., Champion, P. M., Fitchen, D. B., Chiang, R., and Hager, L. P. (1979) *Biochemistry 18*, 2280−2290.
73. Wang, J., Larsen, R., Moench, S. J., Satterlee, J. D., Rousseau, D. L., and Ondrias, M. R. (1996) *Biochemistry 35*, 453−463.
74. Al-Mustafa, J., Sykora, M., and Kincaid, J. R. (1995) *J. Biol. Chem. 270*, 10449−10460.
75. Tsubaki, M., Srivastava, R. B., and Yu, N.-T. (1982) *Biochemistry 21*, 1132−1140.
76. Argade, P. V., Ching, Y. C., and Rousseau, D. L. (1984) *Science 225*, 329−331.
77. Song, S., Boffi, A., Chiancone, E., and Rousseau, D. L. (1993) *Biochemistry 32*, 6330−6336.
78. Kim, S., Deinum, G., Gardner, M. T., Marletta, M. A., and Babcock, G. T. (1996) *J. Am. Chem. Soc. 118*, 8769−8770.
79. O'Keeffe, D. H., Ebel, R. E., Peterson, J. A., Maxwell, J. C., and Caughey, W. S. (1978) *Biochemistry 17*, 5845−5852.
80. Uno, T., Nishimura, Y., Makino, R., Iizuka, T., Ishimura, Y., and Tsuboi, M. (1985) *J. Biol. Chem. 260*, 2023−2026.
81. Jung, C., Hui Bon Hoa, G., Schroder, K.-L., Simon, M., Doucet, J. P. (1992) *Biochemistry 31*, 12855−12862.
82. Wang, J., Wu, C., Ghosh, D. K., Zhang, J., Stuehr, D. J., and Rousseau, D. L. (1996) in *Fifteenth International Conference on Raman Spectroscopy* (Asher, S. A., and Stein, P., Eds.) pp 440−441, John Wiley and Sons, Chichester.
83. Wang, J., Gray, K. A., Daldal, F., and Rousseau, D. L. (1995) *J. Am. Chem. Soc. 117*, 9363−9364.
84. Yu, N.-T., Benko, B., Kerr, E. A., and Gersonde, K. (1984) *Proc. Natl. Acad. Sci. U.S.A. 81*, 5106−5110.
85. Caughey, W. S., Dong, A., Yoshikawa, S., and Zhao, X.-J. (1993) *J. Bioenerg. Biomembr. 25*, 81−92.
86. Wang, J., Ching, Y.-C., Rousseau, D. L., Hill, J. J., Rumbley, J., and Gennis, R. B. (1993) *J. Am. Chem. Soc, 115*, 3390−3391.
87. Garcia-Horsman, J. A., Berry, E., Shapleigh, J. P., Alben, J. O., and Gennis, R. B. (1994) *Biochemistry 33*, 3113−3119.
88. Feldman, M., and McMahon, A. T. (2000) *Ann. Int. Med. 132*, 134−143.
89. Marnett, L. J., and Kalgutkar, A. S. (1999) *Trends Pharmacol. Sci. 20*, 465−469.
90. Spiro, T. G., and Li, X.-Y. (1988) in *Biological Applications of Raman Spectroscopy* (Spiro, T. G., Ed.) Vol. III, pp 1−38, John Wiley and Sons, New York.
91. Reczek, C. M., Sitter, A. J., and Terner, J. (1989) *J. Mol. Struct. 214*, 27−41.

BI001257C